UC Irvine

Title

Synthesis and Evaluation of Compound Targeting α7 and β2 Subunits in Nicotinic Acetylcholinergic Receptor.

Permalink

Journal

Authors

Singh, Karanveer
Ngo, Allyson
Keerthisinghe, Oshini
et al.

Publication Date

DOI

Peer reviewed

Article

Synthesis and Evaluation of Compound Targeting α7 and β2 Subunits in Nicotinic Acetylcholinergic Receptor

Karanveer Singh, Allyson Ngo, Oshini V. Keerthisinghe, Krystal K. Patel, Christopher Liang and Jogeshwar Mukherjee *

Preclinical Imaging, Department of Radiological Sciences, University of California-Irvine, Irvine, CA 92697, USA; karanves@uci.edu (K.S.); allyson1@uci.edu (A.N.); okeerthi@uci.edu (O.V.K.); kkpatel11@gmail.com (K.K.P.); liangc@uci.edu (C.L.)

* Correspondence: mukherjj@hs.uci.edu; Tel.: +1-(949)-824-2018; Fax: +1-(949)-824-2344

Abstract: Nicotinic acetylcholine receptors (nAChRs) are involved in various central nervous system functions and have also been implicated in several neurodegenerative disorders. The heteromeric α4β2* and homomeric α7 are two major nAChR subtypes which have been studied in the brain using positron emission tomography (PET). Our comparative autoradiographic studies of the two receptor types in the mouse and rat brains show major differences in the thalamus (α4β2* >> α7), hippocampus (α7 >> α4β2*), and subiculum (α4β2* >> α7). A relatively newer heteromeric α7β2 nAChR subtype has been identified in the brain which may have a greater role in neurodegeneration. We report the development of KS7 (3-(2-(*S*)-azetidinylmethoxy)-5-(1,4-diaza-bicyclo[3.2.2]nonane)pyridine) which incorporates structural features of Nifzetidine (high affinity for α4β2* nAChR) and ASEM (high affinity for α7 nAChR) in an effort to target α7 and β2 subunits in α7β2 nAChR. KS7 exhibited higher affinities (IC_{50} = 50 to 172 nM) for [^{3}H]cytisine radiolabeled sites and weaker affinities (IC_{50} = 10 μM) for [^{125}I]-α-bungarotoxin radiolabeled rat brain sites in several brain regions. The weaker affinity of KS7 to α7 nAChR may suggest lack of binding at the α7 subunit of α7β2 nAChR. A radiolabeled derivative of KS7 may be required to identify any specific binding to brain regions suggested to contain α7β2 nAChR.

Keywords: [^{18}F]nifene; [^{125}I]α-bungarotoxin; autoradiography; PET; mice; rat; amyloid plaques; α7β2 nAChR

1. Introduction

Neuronal nicotinic cholinergic receptors (nAChRs) are involved in learning, memory, addiction, and neuropsychatric illnesses [1]. Dysfunction of these receptors has been implicated in numerous human conditions including Alzheimer's disease (AD) [2,3], Parkinson's disease (PD) [4], and others. Several nAChR subtypes are present in the mammalian brain, with heteromeric α4β2 and homomeric α7 subtypes being in larger concentrations than the other subtypes ([5,6] Figure 1). Two molecules of acetylcholine (ACh) bind at the interface of α4 and β2 subunits in the α4β2 subtype, while five molecules of ACh bind at the α7-α7 interface in the α7 receptor subtype. Nicotine has a high affinity for the α4β2 subtypes (Ki = 5.45 nM) and is several orders of magnitude weaker for the α7 subtypes (Ki = 223 nM) [7].

Due to the clinical importance of nAChRs, evaluating the activity of these receptors can potentially assist in understanding human illness [8–11]. We have developed several positron emission tomography (PET) imaging agents for non-invasive imaging of high-affinity sites on α4β2* receptors using [^{18}F]nifene [12–15] (Figure 1), [^{18}F]nifrolene [16], and [^{18}F]nifzetidine [17]; for single-photon emission computed tomography (SPECT), [^{123}I]niodene was prepared [18]; and for PET/SPECT, Niofene [19] was examined. For α7 nAChRs, fewer in vivo PET imaging agents are available, with [^{18}F]ASEM being the promi-

nent one [20,21] (Figure 1). For in vitro studies of $\alpha 7$ nAChRs, $[^{125}I]\alpha$-iodobungarotoxin (α-$[^{125}I]$BuTX) binds selectively and has been widely used [22–24].
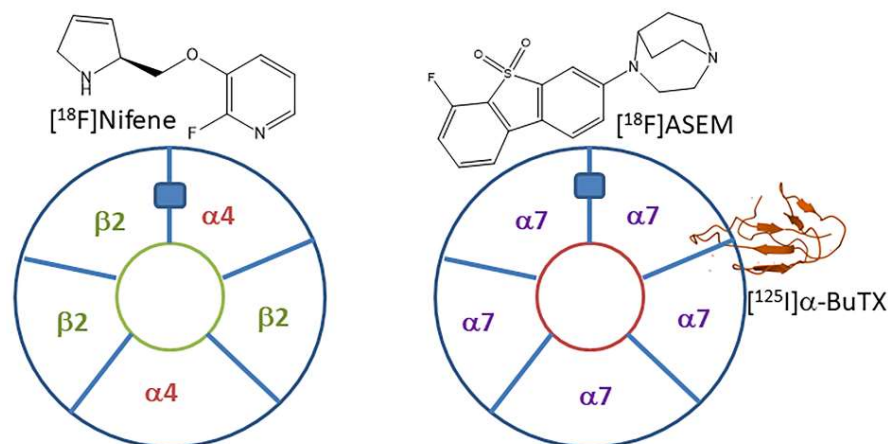

Figure 1. Neuronal nAChRs: Pentameric subunit layout of heteromeric $\alpha 4_2 \beta 2_3$ and homomeric $\alpha 7_5$ nAChRs. The blue rectangle represents one of the acetylcholine sites. At this site, binding of PET radiotracers, $[^{18}F]$nifene ($\alpha 4\beta 2^*$), and $[^{18}F]$ASEM ($\alpha 7$) can occur. Also shown is α-$[^{125}I]$BuTX, binding to homomeric $\alpha 7_5$ nAChRs for autoradiography(structure of α-BuTX from RCSB PDB).

Because cholinergic innervation may be affected in various pathophysiologies, PET and SPECT imaging studies of both $\alpha 4\beta 2^*$ and $\alpha 7$ nAChRs have been underway. Human PET studies and SPECT studies have demonstrated that reduction in binding is implicated in the decline in executive function in AD [25,26]. More recent PET reports [8,9,27] in AD show a decrease in binding in several brain regions and a correlation with cognitive deficits with select brain regions. Results from the limited PET studies of $\alpha 7$ receptors have been mixed, suggesting an increase in mild cognitive impairment (MCI) and no change in AD [28]. Further studies are needed to ascertain the role of $\alpha 7$ receptors because of their higher concentration in the hippocampus, a region inflicted with AD pathology of Aβ plaques and neurofibrillary tangles [29].

More recently, heteromeric $\alpha 7\beta 2$ nAChR subtype has been isolated and characterized in the mammalian forebrain [30–33]. Distribution of $\alpha 7\beta 2$ subtype was found to be greater in the rodent basal forebrain cholinergic neurons and hippocampal interneurons and in human cerebral cortex neurons. However, the overall brain distribution and relative concentration of this new subtype (compared to $\alpha 4\beta 2$ and $\alpha 7$ subtypes) is yet to be determined. In addition, functional properties of the $\alpha 7\beta 2$ nAChR are yet to be fully understood. Compared to the $\alpha 7$ receptors, the $\alpha 7\beta 2$ subtype displays greater sensitivity to oligomeric amyloid β peptide (Aβ) and this interaction between Aβ and $\alpha 7\beta 2$ nAChR may be relevant in the pathogenesis of AD [2,34]. Since the $\alpha 7\beta 2$ nAChR is pharmacologically distinct from the homomeric $\alpha 7$ nAChR, it likely plays a unique functional role in the mammalian brain. For these reasons, pursuit of a PET imaging agent for the $\alpha 7\beta 2$ nAChR may be a worthwhile goal. However, considering the lower concentrations and structural similarities of the receptor subtypes, it remains to be determined if this a feasible target.

Two heteropentameric subtypes, $\alpha 7_4 \beta 2_1$ ($\alpha 7$-$\alpha 7$-$\alpha 7$-$\alpha 7$-$\beta 2$) and $\alpha 7_3 \beta 2_2$ ($\alpha 7$-$\beta 2$-$\alpha 7$-$\beta 2$-$\alpha 7$), have been identified ([32]; Figure 2). No agonists or antagonists which bind to $\alpha 7$ subtype or $\alpha 4\beta 2$ subtype have yet been identified to show selectivity for $\alpha 7\beta 2$ subtype. It is not known if the ligand binding occurs at the $\alpha 7$-$\alpha 7$ interface or $\alpha 7$-$\beta 2$ interface. Binding of α-$[^{125}I]$BuTX occurs at the $\alpha 7$-$\alpha 7$ interface and therefore, it is unclear if it would bind to the $\alpha 7$-$\beta 2$ interface [35]. It is also not known if α-$[^{125}I]$BuTX would be able to identify the heteromeric $\alpha 7_4 \beta 2$ and $\alpha 7_3 \beta 2_2$ nAChRs since they have the $\alpha 7$-$\alpha 7$ interfaces as well as $\alpha 7$-$\beta 2$ interfaces.
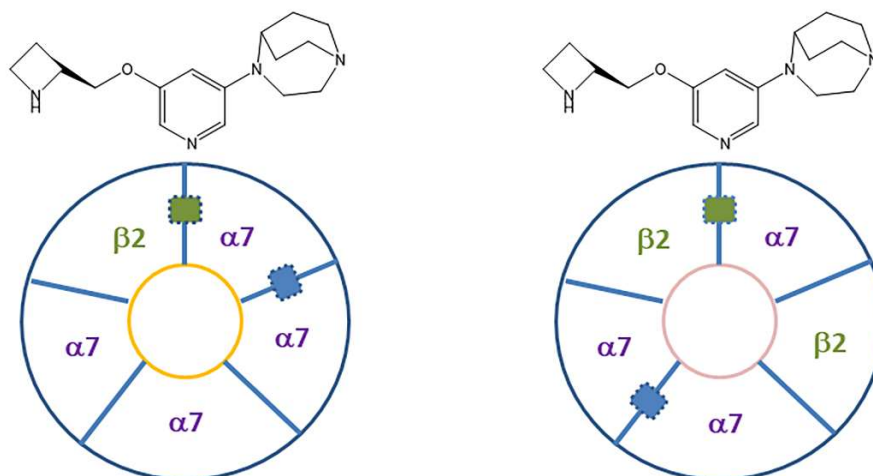
Figure 2. $\alpha7\beta2$ Pentameric subunits layout: Heteromeric $\alpha7_4\beta2_1$ and $\alpha7_3\beta2_2$ nAChRs. The blue rectangle represents one of the potential $\alpha7$-$\alpha7$ interface binding sites. At this site, binding of KS7 may occur with the with the 1,4-diaza-bicyclo[3.2.2]nonane binding towards $\alpha7$. It is suggested that $\beta2$ (green rectangle) may be a secondary binding site.

In an effort to identify a potential $\alpha7\beta2$ ligand, we have chosen features of nifzetidine (Figure 3, **4**), a high affinity $\alpha4\beta2$ ligand previously developed in our laboratories [17] and those of $\alpha7$ agonists developed by Abbott laboratories [36] and ASEM ([20] Figure 3, **3**). The azetidine feature from nifzetidine which potentially binds to the $\beta2$ subunit and the 1,4-diaza-bicyclo[3.2.2]nonane feature from ASEM which potentially binds to the $\alpha7$ subunit were both incorporated into KS7 (Figure 3, **5**) in an effort to bind to the $\alpha7$-$\beta2$ interface.
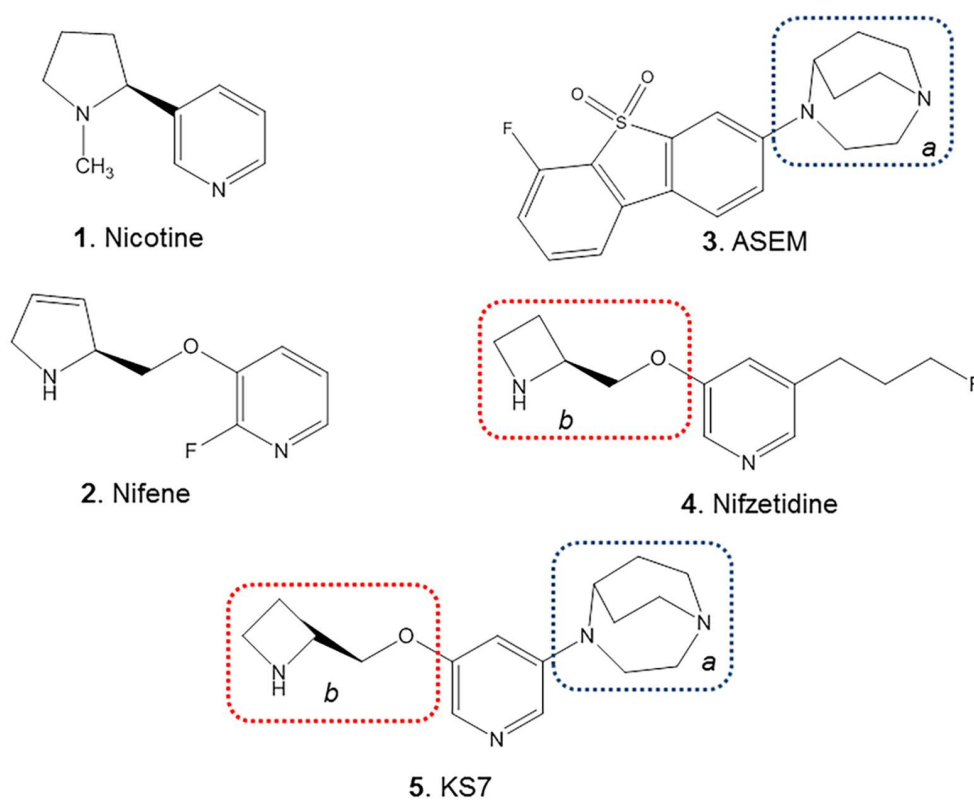
Figure 3. Chemical structures of PET Radiotracers: Heteromeric $\alpha4_2\beta2_3$ (nicotine, nifene, nifzetidine) and homomeric $\alpha7_5$ (ASEM) nAChRs. Proposed structure (KS7) for heteromeric $\alpha7_4\beta2$ and $\alpha7_3\beta2_2$ nAChRs incorporates the 1,4-diaza-bicyclo[3.2.2]nonane ring (blue dotted box) from ASEM (binds to $\alpha7$) and azetidinylmethoxy ring (red dotted box) from Nifzetidine (binds to $\alpha4\beta2$).

Thus, in this paper, we report the following: (1) synthesis and characterization of 3-(2-(*S*)-azetidinylmethoxy)-5-(1,4-diaza-bicyclo[3.2.2]nonane)pyridine (KS7, Figure 4, **5**); (2) measurement of in vitro binding affinities of KS7 using [³H]cytisine to label the $\alpha4\beta2^*$ nAChR sites; and (3) measurement of in vitro binding affinities KS7 in rat brain slices using α-[¹²⁵I]BuTX to label the $\alpha7$ nAChR sites.
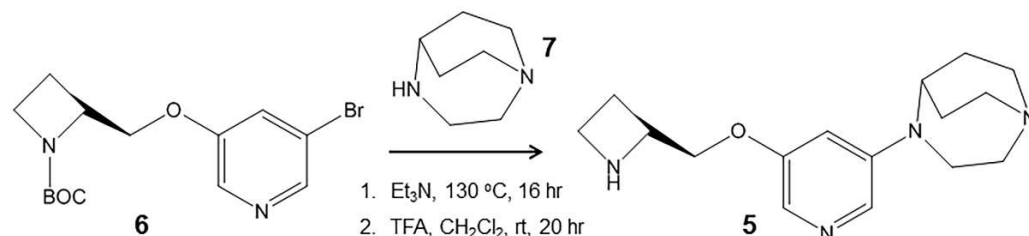
**Figure 4.** Synthesis: reaction scheme for synthesis of KS7 (**5**).

2. Results and Discussion

Distribution of $\alpha4\beta2^*$ and $\alpha7$ nAChRs, two major receptor subtypes in the mammalian brain have been well-studied. Our studies on the distribution of the two receptor subtypes, $\alpha4\beta2^*$ and $\alpha7$ nAChRs, in mice and rat brains show distinct areas of similarities and differences (Figure 5). Using [¹⁸F]nifene for $\alpha4\beta2^*$ nAChRs, the ratio versus cerebellum (used as a reference region) for rat brains was in the order of thalamus > subiclum > striatum > frontal cortex > superior colliculus > inferior colliculus > hippocampus > cerebellum [12,13]. Similar binding profile was observed in the rat brains using [³H]cytisine [37]. The mice brains generally exhibited higher ratios compared to rats for [¹⁸F]nifene-labeled $\alpha4\beta2^*$ nAChRs.

Using α-[¹²⁵I]BuTX for $\alpha7$ nAChRs, the ratio versus cerebellum (used as a reference region) for rat brains was in the order of hippocampus > inferior colliculus > frontal cortex > superior colliculus > subiculum > thalamus > striatum > cerebellum similar to previous reports for $\alpha7$ nAChRs [21,24]. Some minor differences in the inferior and superior colliculi were observed between mouse and rat brains for $\alpha7$ nAChRs.

These comparative autoradiographic studies of the two receptor types in the mouse and rat brains show major differences in the thalamus ($\alpha4\beta2^* \gg \alpha7$) and hippocampus ($\alpha7 \gg \alpha4\beta2^*$). Also noteworthy is the difference in subiculum ($\alpha4\beta2^* \gg \alpha7$). The colliculi (superior and inferior) exhibited presence of both $\alpha4\beta2^*$ and $\alpha7$ nAChRs, the latter appeared to be more discreet. The regional distribution of α-[¹²⁵I]BuTX is comparable to the binding of the small molecule ASEM [21]. Similar to these findings in the rodents, human studies with $\alpha4\beta2^*$ and $\alpha7$ nAChRs PET radiotracers have been reported. In the case of $\alpha4\beta2^*$ nAChRs, our comparative study of [¹⁸F]nifene across different species suggest a high degree of homology [7]. In the case of $\alpha7$ nAChRs PET using [¹⁸F]ASEM, similarity across species has been reported [38].

In all species, there are a number of brain regions where there is some overlap between $\alpha7$ and $\beta2$ nAChRs subunits [39–41]. Thus, heteromeric $\alpha7\beta2$ nAChR subtype has been isolated and characterized and was found to be greater in the basal forebrain cholinergic neurons and hippocampal interneurons and in human cerebral cortex neurons [30–33]. Regional brain distribution and relative concentration of this new subtype is yet to be determined. The $\alpha7\beta2$ subtype may be more sensitive to oligomeric Aβ peptide and this interaction between Aβ and $\alpha7\beta2$ nAChR may be relevant in the pathogenesis of AD [2,34]. Since the heteromeric $\alpha7\beta2$ nAChR is likely pharmacologically distinct from the homomeric $\alpha7$ nAChR, a selective radioligand for imaging is necessary to study its distribution in the brain. Efforts have been made to assess [¹²⁵I]α-BuTX binds to $\alpha7\beta2$ nAChR [31,32]. Other $\alpha7$ and $\alpha4\beta2^*$ drugs have not been shown to clearly differentiate between $\alpha7$ and $\alpha7\beta2$ nAChRs [32]. For these reasons, pursuit of a drug compound for the $\alpha7\beta2$ nAChR may be a worthwhile goal. If found selective, this drug could then be radiolabeled for imaging studies. Towards this goal, we designed and synthesized KS7 (Figures 3 and 4) which is incorporated structural components of Nifzetidine ($\alpha4\beta2^*$ nAChR) and ASEM ($\alpha7$ nAChR).
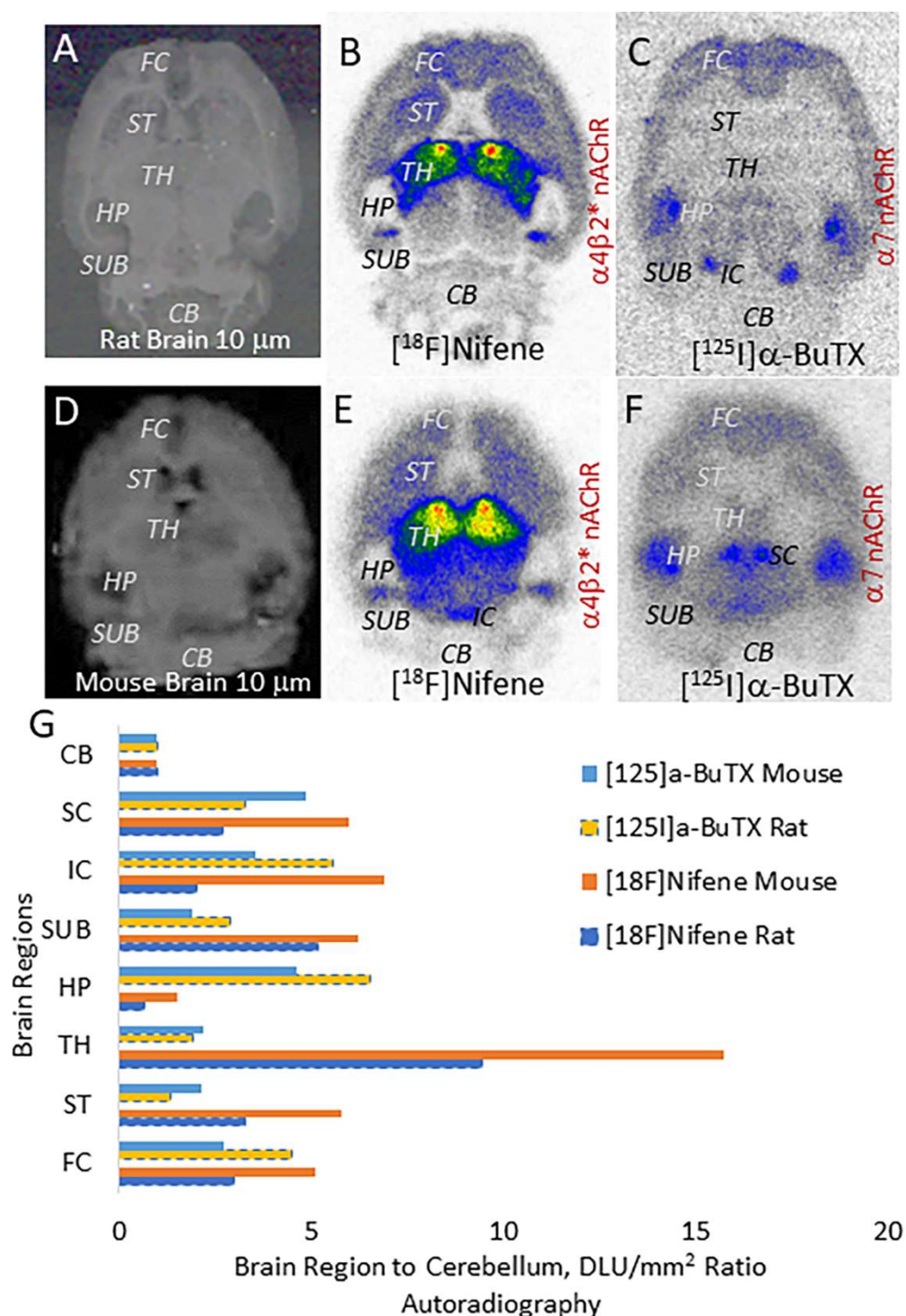
Figure 5. Autoradiography of α4β2 and α7 nAChRs: (**A–C**): Rat brain slices; (**A**) scan of 10 μm thick horizontal rat brain slice showing different regions; (**B**) binding of [^{18}F]nifene to α4β2* nAChRs in the rat brain slice with highest binding in TH; (**C**) binding of α-[^{125}I]BuTX to α7 nAChRs in rat brain slice with highest binding in HP. (**D–F**): Mouse brain slices; (**D**) scan of 10 μm thick horizontal mouse brain slice showing different regions; (**E**) binding of [^{18}F]nifene to α4β2* nAChRs in mouse brain slice with highest binding in TH; (**F**) binding of α-[^{125}I]BuTX to α7 nAChRs in mouse brain slice with highest binding in HP. (**G**) Comparison of ratios of brain regions to cerebellum in rat and mouse brain for [^{18}F]nifene and α-[^{125}I]BuTX (CB—cerebellum; SC—superior colliculus; IC—inferior colliculus; SUB—subiculum; HP—hippocampus; TH—thalamus; ST—striatum; FC—frontal cortex).

In vitro binding affinity studies of KS7 were carried out on rat brain slices labeled with [³H]cytisine (Figure 6). Figure 6A shows [³H]cytisine labeling of rat brain regions of thalamus, frontal cortex, anterior cingulate, striatum, subiculum, and cerebellum as previously reported [37]. With increasing concentration of KS7, binding of [³H]cytisine was reduced from all brain regions.
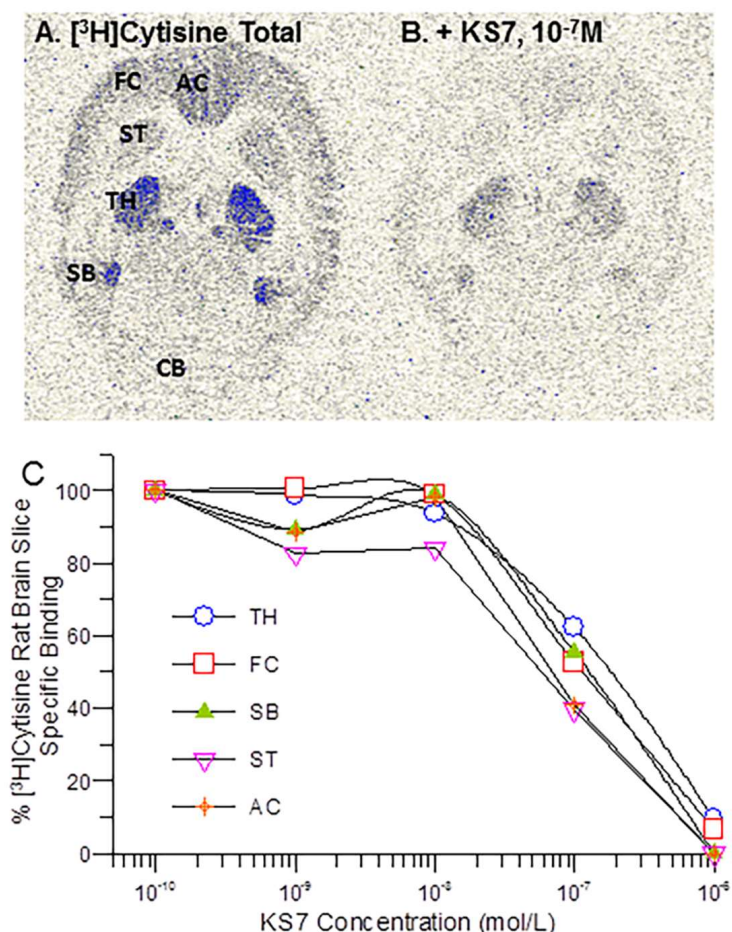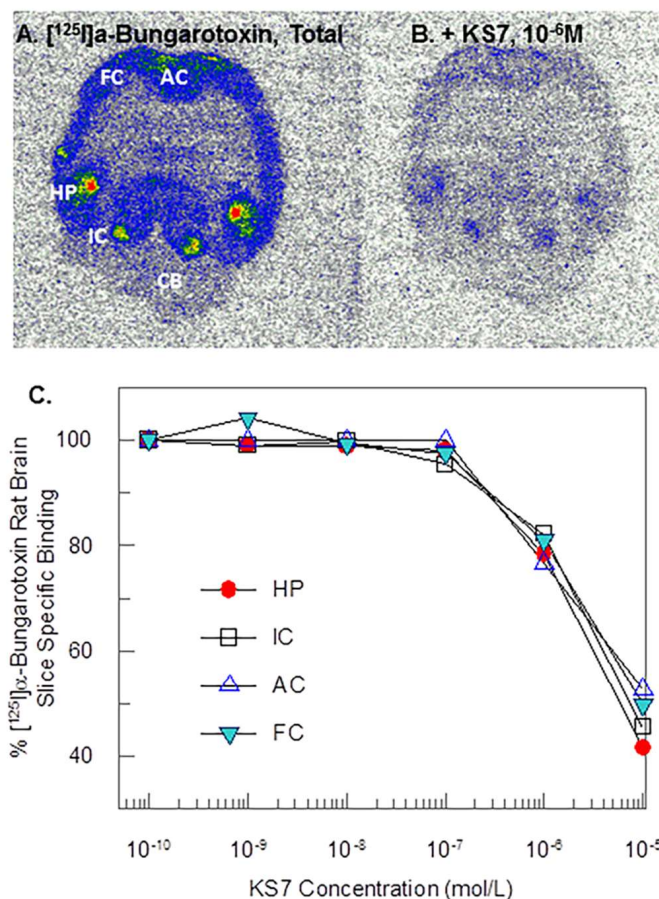

Figure 6. α4β2 Binding Affinity: Binding affinity of [³H]cytisine in the presence of KS7 on rat brain regions. (**A**) Total binding of [³H]cytisine in different brain regions (AC—anterior cingulate; FC—frontal cortex; ST—striatum; TH—thalamus; SB—subiculum; CB—cerebellum); (**B**) binding of rat brain slice at 10^{-7} M. (**C**) Competition binding curves of rat brain slices shown in (**A**,**B**).

Measured inhibitory constants (IC$_{50}$) of KS7 in the various brain regions were: striata = 86.9 nM; frontal cortex = 109 nM; thalamus = 134 nM; subiculum = 172 nM; anterior cingulate = 49.5 nM (Table 1).

Table 1. Inhibition constants (IC$_{50}$) for KS7 at nicotinic receptors.

Brain Region	[³H]Cytisine, α4β2* nAChRs	[¹²⁵I]α-BuTX, α7* nAChRs	α7/α4β2 Ratio
Thalamus	1.34×10^{-7}	-	-
Frontal Cortex	1.09×10^{-7}	9.90×10^{-6}	91
Anterior Cingulate	4.95×10^{-8}	1.26×10^{-5}	254
Subiculum	1.72×10^{-7}	-	-
Striatum	8.69×10^{-8}	-	-
Hippocampus	-	3.32×10^{-5}	-
Inferior Colliculus	-	4.68×10^{-5}	-

For $\alpha 7$ nAChRs, Figure 7 shows [^{125}I]α-BuTX labeling of rat brain regions of frontal cortex, anterior cingulate, hippocampus, inferior colliculus, and cerebellum. With increasing concentration of KS7, binding of α-[^{125}I]BuTX was reduced from all brain regions. Measured inhibitory constants (IC$_{50}$) of KS7 in the various brain regions were frontal cortex = 9.9 μM; anterior cingulate = 12.6 μM; hippocampus = 33.2 μM; and inferior colliculus = 46.8 μM. The selectivity of KS in frontal cortex and anterior cingulate was in favor of $\alpha 4 \beta 2^*$ nAChR subtype.


Figure 7. $\alpha 7$ Binding affinity: binding affinity of α-[^{125}I]BuTX in the presence of KS7 on rat brain regions. (**A**) Total binding of α-[^{125}I]BuTX in different brain regions (FC—frontal cortex; AC—anterior cingulate; HP—hippocampus; IC—inferior colliculus; CB—cerebellum); (**B**) binding of rat brain slice at 10^{-6} M. (**C**) Competition binding curves of rat brain slices shown in (**A**,**B**).

Based on the crystal structure of the $\alpha 4 \beta 2^*$ receptor [42], the high-affinity binding sites sit at the interface between the $\alpha 4$ and $\beta 2$ subunits in the receptor complex. Binding of the azetidine ring nitrogen is likely at the $\alpha 4$ subunit side and since this part of the molecule remains the same in the case of KS7, moderate affinity for the $\alpha 4 \beta 2^*$ receptor sites is maintained. Figure 8 shows similarity of energy minimized structures of nifzeridine and KS7 in the overlay (Figure 8D,E). The presence of the azabicylononane ring may be causing a decrease in the affinity at the $\alpha 4 \beta 2^*$ receptor. Significant deviation in the overlay structures of ASEM and KS7 is seen (Figure 8F,G) which may be the reason for the larger decrease in the affinity at the $\alpha 7$ receptor sites. This may be favorable in terms of directing KS7 away from the $\alpha 7$ nAChRs.

Table 2 summarizes the affinities and selectivities for the various at the $\alpha 4 \beta 2$ and $\alpha 7$ nAChRs. The selectivity of KS7 seems to resemble nicotine, as a dual $\alpha 4 \beta 2 / \alpha 7$ drug [43], but with significantly weaker affinities compared to nicotine.
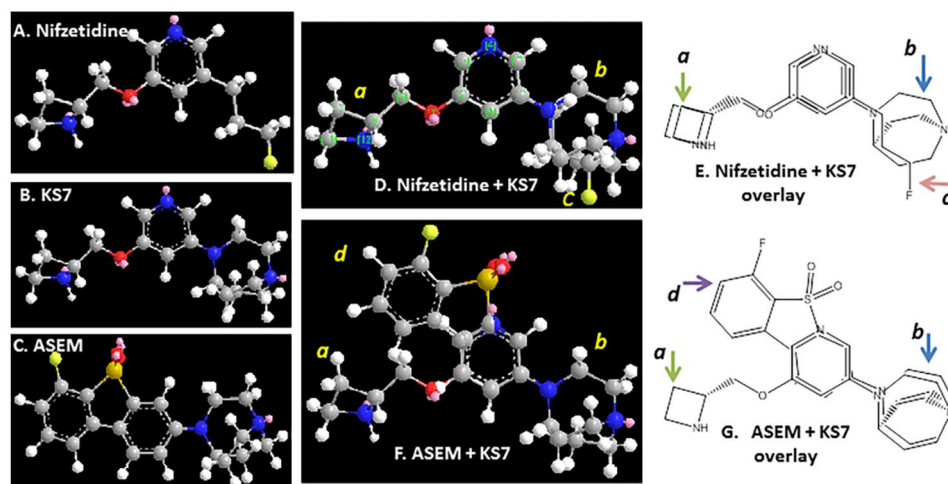
Figure 8. KS7 Structure comparisons: (**A**) minimized energy structure of nifzetidine with reported high affinity for α4β2* receptors; (**B**) minimized energy structure of KS7; (**C**) energy minimized structure of ASEM with reported high affinity for α7 nAChR. (**D,E**) Minimized energy structure and chemical structure of nifzetidine and KS7 overlay; (**F,G**) minimized energy structure and chemical structure of ASEM with KS7 overlay.

Table 2. Binding affinities of various drugs for α4β2 and α7 nAChRs.

Drug	α4β2*, nM	α7*, nM	α7/α4β2 Ratio	α4β2/α7 Ratio
Nicotine	6.93 [a] 1.68 [b]	223 [c]	32 133	0.03
Nifene	1.07 [a] 0.50 [b]	169 [c]	158 338	0.007
Cytisine	1.51 [d] 1.27 [e]	691 [e]	544 [e]	0.002
α-Iodobungarotoxin	>1000 [f]	0.50 [g]	0.0005	2000
IodoASEM ASEM	1707 [h] 562 [i]	0.5 [h] 0.37 [i]	0.0003 0.0007	3414 [h] 1370 [i]
KS7	109 [j]	9900 [j]	91 [j]	0.01 [j]

[a] Rat brain cortex labeled with ^{3}H-epibatidine [7]. [b] Rat brain homogenates labeled with ^{3}H-cytisine [12]. [c] Rat cloned receptors labeled with α-[^{125}I]BuTX [7]. [d] Cytisine tested in rat [44]; [e] Cytisine tested on heterologously expressed human receptors; α4β2 in HEK293 cells and α7 nAChR in SH-SY5Y human neuroblastoma cells [45]. [f] [^{3}H]nicotine inhibition by α-bungarotoxin [46]; [g] α-iodobungarotoxin tested in rat [41]; [h] Iodo-ASEM affinities HEK293 membranes expressing α7 and α4β2 nAChRs [47]; [i] HEK293 cells transfected with α7 and α4β2 nAChRs [48]; [j] Frontal cortex values for KS7 taken from Table 1.

3. Materials and Methods

3.1. General Methods

All chemicals and solvents were of analytical or HPLC grade from Aldrich Chemical Co. and Fisher Scientific. Electrospray mass spectra were obtained on a Model 7250 mass spectrometer (Micromass LCT, Milford, MA, USA). Proton NMR spectra were recorded on a Bruker OMEGA 600 MHz spectrometer. Analytical thin layer chromatography (TLC) was carried out on silica-coated plates (Baker-Flex, Phillipsburg, NJ, USA). Chromatographic separations were carried out on preparative TLC (silica gel GF 20 × 20 cm, 2 mm thick; Alltech Assoc. Inc., Deerfield, IL, USA) or silica gel flash columns or semi-preparative reverse-phase columns using the Gilson high-performance liquid chromatography (HPLC) systems. [^{3}H]cytisine and α-[^{125}I]BuTX, purchased from American Radiolabeled Chemicals, Inc., St Louis MO, were used for autoradiographic studies by exposing tissue samples on storage phosphor screens. The apposed phosphor screens were read and analyzed by

OptiQuant acquisition and analysis program of the Cyclone Storage Phosphor System (Packard Instruments Co., Boston, MA, USA).

3.2. Animals

All animal studies were approved by the Institutional Animal Health Care and Use Committee (IACUC) of University of California-Irvine. Adult male Sprague Dawley rats (*n* = 4) were used in this study (280 g; 18–24 weeks). Rats were purchased from Jackson Laboratory. Adult male C57BL/6 mice were used in this study (28 g). Mice were purchased from Jackson Laboratory. All animals were housed under controlled temperatures of 22 °C ± 1 °C, in a 12 h light–dark cycle, on at 6:00 AM, with water and food chow ad libitum. Brains from the mice and rats were excised, and horizontal slices were prepared at 10 µm thickness using a Leica 1850 cryotome at −20 °C. The brain slices containing the cortex, striatum, thalamus, hippocampus, and cerebellum were stored in −80 °C freezer and used for binding studies.

3.3. Synthesis

(3-(2-(*S*)-azetidinylmethoxy)-5-(1,4-diazabicyclo[3.2.2]nonane)pyridine) (Figure 4, **5**; KS7): 3-Bromo-5-(1-*tert*-butoxycarbonyl-2-(*S*)-azetidinylmethoxy)pyridine (Figure 4, **6**) (34 mg; 0.1 mmol) was dissolved in triethylamine (0.1 mL). To this solution, 1,4-diazabicyclo[3.2.2]nonane (15 mg; 0.12 mmol) was added and the closed reaction 10 mL V-vial was heated at 130 °C for 16 h. The reaction mixture was purified on preparative silica gel TLC using 9:1 dichloromethane-methanol to provide of pure (3-(1-*tert*-butoxycarbonyl-2-(*S*)-azetidinylmethoxy)-5-(1,4-diazabicyclo[3.2.2]nonane)pyridine). Mass spectra (*m/z*, %): 389 ([M + H]$^+$, 10%), 411 ([M + Na]$^+$, 80%). We anticipated this reaction to be sluggish and low-yielding (due to the 3-bromo position in the pyridine ring). The *N*-BOC intermediate was obtained in <5% yield. Prolonged reaction time was not useful in increasing the yield. Deprotection of the N-*tert*-butoxycarbonyl was carried out by treatment with trifluoroacetic acid (TFA; 0.1 mL) in dichloromethane (1 mL) at room temperature or 24 h. The final product, (3-(2-(*S*)-azetidinylmethoxy)-5-(1,4-diazabicyclo[3.2.2]-nonane)pyridine) (Figure 4, **5**, KS7) was obtained by preparative TLC (1:1 dichloromethane-methanol) in <5% overall yield. Removal of the *N*-BOC protecting group using trifluoroacetic acid resulted in KS7 which was isolated as a KS7 trifluoroacetate salt was used for in vitro studies. Mass spectra (*m/z*, %): 312 ([M + Na]$^+$, 100%); 1H NMR (CDCl$_3$, 600 MHz) δ ppm: 8.28 (m, 2H), 7.43 (dd, J = 1.8, 2.6 Hz, 1H), 4.33 (m, 1H), 4.13 (m, 4H), 3.89 (m, 2H), 3.60 (m, 2H), 3.20 (m, 4H), 2.95 (m, 2H), 2.33 (m, 2H), 2.20 (m, 2H), 1.95 (m, 2H).

3.4. In Vitro Autoradiographic Studies α4β2* nAChR—[^{18}F]Nifene

Autoradiography of [^{18}F]nifene in mice and rat brain slices were previously reported [3,12]. Briefly, slides with brain slices were incubated with [^{18}F]nifene in a Tris buffer pH 7.4 (60 mL; 37 kBq/mL) and was added to the chambers and were incubated at 25 °C for 1 h. Nonspecific binding was measured in separate chambers in the presence of 300 µM nicotine. The slices were then washed with cold buffer twice, 3 min each time, Tris buffer, and cold water for rinse. The brain sections were air dried, exposed overnight on a phosphor film, and then placed on the Phosphor Autoradiographic Imaging System/Cyclone Storage Phosphor System (Packard Instruments Co.). Regions of interest (ROIs) were drawn on the slices and the extent of binding of [^{18}F]nifene was measured in Digital Light Units/mm^2 (DLU/mm^2) using the OptiQuant acquisition and analysis program (Packard Instruments Co.).

3.5. In Vitro Binding Affinity Studies α4β2* nAChR—[^{3}H]Cytisine

Our previously published procedures were used for [^{3}H]cytisine experiments [37]. Horizontal brain slices, 10 µm thick from male Sprague Dawley rats, were preincubated in the buffer (50 mmol/L Tris HCl containing 120 mmol/L NaCl, 5 mmol/L KCl, 2.5 mmol/L CaCl$_2$, 1 mmol/L MgCl$_2$, pH 7.4) for 10 min. The pre-incubation buffer was then discarded and the slices were incubated with [^{3}H]cytisine (2.5 nM, specific activity of 32.7 Ci/mmol)

at 2 °C for 75 min. Binding was measured in the presence of 0.1 nM to 1 μM of KS7 and 300 μM of nicotine was used for nonspecific binding. After incubation, slices were washed twice (2 min each wash) with ice-cold Tris buffer, pH 7.4, followed by a quick rinse in cold (0–5 °C) deionized water. The slides were then air dried and the radiolabeled brain sections were apposed on storage phosphor screens for two weeks (Perkin Elmer Multisensitive, Medium MS, New Jersy, USA). For autoradiographic analysis, the apposed phosphor screens were read and analyzed by OptiQuant acquisition and analysis program of the Cyclone Storage Phosphor System (Packard Instruments Co., Boston, MA, USA). Regions of interest of same size were drawn and analyzed on brain regions using OptiQuant software version 2 and binding of [^{3}H]cytisine measured in DLU/mm^2. Data were analyzed using following procedure: (a) the non-specific binding of [^{3}H]cytisine was subtracted for all samples; (b) the specific binding was normalized to 100% (no competitive ligand); and (c) the binding isotherms were fit to the Hill equation (KELL BioSoft software (v 6), Cambridge, UK).

3.6. In Vitro Autoradiographic Studies α7 nAChR—α-[^{125}I] BuTX

Autoradiography of α-[^{125}I]BuTX in mice and rat brain slices were previously reported [21,24]. The horizontal brain slices were preincubated in 50 mM Tris HCl, pH 7.3, containing 0.1% bovine serum albumin (BSA) at room temperature for 30 min. After the preincubation, the slices were incubated with α-[^{125}I]BuTX (0.2 nM, specific activity of 2200 Ci/mmol) at room temperature for 120 min. Nonspecific binding was measured in separate chambers in the presence of 300 μM nicotine. After incubation, slices were washed three times (10 min each wash) with ice-cold Tris buffer, pH 7.3, followed by a quick rinse in cold (0–5 °C) deionized water. The brain sections were air dried, exposed for a week on a phosphor film, and then placed on the Phosphor Autoradiographic Imaging System/Cyclone Storage Phosphor System (Packard Instruments Co.). Regions of interest (ROIs) were drawn on the slices and the extent of binding of [^{125}I]α-bungarotoxin was measured in DLU/mm^2 using the OptiQuant acquisition and analysis program (Packard Instruments Co.).

3.7. In Vitro Binding Affinity Studies α7 nAChR—[^{125}I]α-Bungarotoxin

For the α-[^{125}I]BuTX assay, the reported method was used [24]. The horizontal rat brain slices were preincubated in 50 mM Tris HCl, pH 7.3, containing 0.1% bovine serum albumin (BSA) at room temperature for 30 min. The pre-incubation buffer was then discarded and the slices were incubated with α-[^{125}I]BuTX (0.2 nM, specific activity of 2200 Ci/mmol) at room temperature for 120 min. Binding was measured in the presence of 0.1 nM to 1 μM of KS7 and 300 μM of nicotine was used for nonspecific binding. After incubation, slices were washed three times (10 min each wash) with ice-cold Tris buffer, pH 7.3, followed by a quick rinse in cold (0–5 °C) deionized water. The slides were then air dried and the radiolabeled brain sections were apposed on storage phosphor screens for one week (Perkin Elmer Multisensitive, Medium MS). For autoradiographic analysis, the apposed phosphor screens were read and analyzed by OptiQuant acquisition and analysis program of the Cyclone Storage Phosphor System (Packard Instruments Co., Boston, MA, USA).

Regions of interest of same size were drawn and analyzed on brain regions using OptiQuant software and binding of α-[^{125}I]BuTX measured in digital light units/mm^2 (DLU/mm^2). Data were analyzed using following procedure: (a) the non-specific binding of α-[^{125}I] BuTX was subtracted for all samples; (b) the specific binding was normalized to 100% (no competitive ligand); and (c) the binding isotherms were fit to the Hill equation (KELL BioSoft software (v 6), Cambridge, UK).

4. Conclusions

Heteromeric α4β2 and homomeric α7 nAChR subtypes have well-defined brain distribution patterns across the various species. A relatively new heteromeric α7β2 nAChR has been identified for which there is currently no selective drug or imaging agent. A new

compound, KS7 has been synthesized as a potential candidate that may bind to the α7 and β2 subunits. The moderate to weak affinities of KS7 to α4β2 and α7 sites is promising. Cell lines expressing the α7β2 nAChRs will be necessary to assess selectivity in binding. A radiolabeled derivative of KS7 using fluorine-18 or carbon-11 labeling either directly on the pyridine ring or other strategies is planned [12,16,49,50]. This may enable autoradiographic studies to identify any discreet binding to hippocampal regions or the forebrain regions, where α7β2 nAChRs may be present. Imaging studies related to the association of Aβ plaque with nAChR subtypes will provide useful information on the potential role of this interaction in AD transgenic mice models [3,51].

References

1. Valles, A.S.; Barrantes, F.J. Nicotinic acetylcholine receptor dysfunction in addiction and in some neurodegenerative and neuropsychiatric disease. *Cells* **2023**, *12*, 2051. [CrossRef] [PubMed]
2. Lombardo, S.; Maskos, U. Role of the nicotinic acetylcholine receptor in Alzheimer's disease pathology and treatment. *Neuropharmacology* **2015**, *96 Pt B*, 255–262. [CrossRef] [PubMed]
3. Liang, C.; Nguyen, G.A.; Danh, T.B.; Sandhu, A.K.; Melkonyan, L.L.; Syed, A.U.; Mukherjee, J. Abnormal [18F]NIFENE binding in transgenic 5xFAD mouse model of Alzheimer's disease: In vivo PET/CT imaging studies of α4β2* nicotinic acetylcholinergic receptors and in vitro correlations with Aβ plaques. *Synapse* **2023**, *77*, e22265. [CrossRef] [PubMed]
4. Campoy, A.T.; Liang, C.; Ladwa, R.M.; Patel, K.K.; Patel, I.H.; Mukherjee, J. [18F]Nifene PET/CT Imaging in Mice: Improved Methods and Preliminary Studies of α4β2* Nicotinic Acetylcholinergic Receptors in Transgenic A53T Mouse Model of α-Synucleinopathy and Post-Mortem Human Parkinson's Disease. *Molecules* **2021**, *26*, 7360. [CrossRef] [PubMed]
5. Taly, A.; Corringer, P.J.; Guedin, D.; Lestage, P.; Changeux, J.P. Nicotinic receptors: Allosteric transitions and therapeutic targets in the nervous system. *Nat. Rev. Drug Discov.* **2009**, *8*, 733–750. [CrossRef] [PubMed]
6. Ho, T.N.T.; Abraham, N.; Lewis, R.J. Structure-Function of Neuronal Nicotinic Acetylcholine Receptor Inhibitors Derived from Natural Toxins. *Front. Neurosci.* **2020**, *14*, 609005. [CrossRef] [PubMed]
7. Mukherjee, J.; Lao, P.J.; Betthauser, T.J.; Samra, G.K.; Pan, M.L.; Patel, I.H.; Liang, C.; Metherate, R.; Christian, B.T. Human brain imaging of nicotinic acetylcholine α4β2* receptors using [18F]Nifene: Selectivity, functional activity, toxicity, aging effects, gender effects, and extrathalamic pathways. *J. Comp. Neurol.* **2018**, *526*, 80–95. [CrossRef]
8. Sabri, O.; Meyer, P.M.; Gräf, S.; Hesse, S.; Wilke, S.; Becker, G.A.; Rullmann, M.; Patt, M.; Luthardt, J.; Wagenknecht, G.; et al. Cognitive correlates of α4β2 nicotinic acetylcholine receptors in mild Alzheimer's dementia. *Brain* **2018**, *141*, 1840–1854. [CrossRef]
9. Sultzer, D.L.; Melrose, R.J.; Riskin-Jones, H.; Narvaez, T.A.; Veliz, J.; Ando, T.K.; Juarez, K.O.; Harwood, D.G.; Brody, A.L.; Mandelkern, M.A. Cholinergic Receptor Binding in Alzheimer Disease and Healthy Aging: Assessment In Vivo with Positron Emission Tomography Imaging. *Am. J. Geriatr. Psychiatry* **2017**, *25*, 342–353. [CrossRef]
10. Quik, M.; Bordia, T.; Zhang, D.; Perez, X.A. Nicotine and Nicotinic Receptor Drugs: Potential for Parkinson's Disease and Drug-Induced Movement Disorders. *Int. Rev. Neurobiol.* **2015**, *124*, 247–271.
11. Perez-Lloret, S.; Barrantes, F.J. Deficits in cholinergic neurotransmission and their clinical correlates in Parkinson's disease. *NPJ Park. Dis.* **2016**, *2*, 16001. [CrossRef] [PubMed]

12. Pichika, R.; Easwaramoorthy, B.; Collins, D.; Christian, B.T.; Shi, B.; Narayanan, T.K.; Potkin, S.G.; Mukherjee, J. Nicotine α4β2* receptor imaging agents. Part II. Synthesis and biological evaluation of 2-[18F]fluoro-3-[2-(*S*)-pyrrolinyl-3,4-dehydromethoxy]pyridine (18F-Nifene) in rodents and imaging by PET in non-human primate. *Nucl. Med. Biol.* **2006**, *33*, 295–304. [CrossRef] [PubMed]

13. Bieszczad, K.M.; Kant, R.; Constantinescu, C.C.; Pandey, S.K.; Kawai, H.D.; Metherate, R.; Weinberger, N.M.; Mukherjee, J. Nicotinic acetylcholine receptors in rat forebrain that bind 18F-nifene: Relating PET imaging, autoradiography, and behavior. *Synapse* **2012**, *66*, 418–434. [CrossRef] [PubMed]

14. Kant, R.; Constantinescu, C.C.; Parekh, P.; Pandey, S.K.; Pan, M.L.; Easwaramoorthy, B.; Mukherjee, J. Evaluation of F-nifene binding to α4β2 nicotinic receptors in the rat brain using microPET imaging. *EJNMMI Res.* **2011**, *1*, 6. [CrossRef] [PubMed]

15. Lao, P.J.; Betthauser, T.J.; Tudorascu, D.L.; Barnhart, T.E.; Hillmer, A.T.; Stone, C.K.; Mukherjee, J.; Christian, B.T. [18F]Nifene test-retest reproducibility in first-in-human imaging of α4β2* nicotinic acetylcholine receptors. *Synapse* **2017**, *71*, e21981. [CrossRef]

16. Pichika, R.; Kuruvilla, S.A.; Patel, N.; Vu, K.; Sinha, S.; Easwaramoorthy, B.; Narayanan, T.K.; Shi, B.; Christian, B.; Mukherjee, J. Nicotinic α4β2 receptor imaging agents. Part IV. Synthesis and biological evaluation of 3-(2-(S)-3,4-dehydropyrrolinyl methoxy)-5-(3′-18F-fluoropropyl)pyridine (18F-Nifrolene) using PET. *Nucl. Med. Biol.* **2013**, *40*, 117–125. [CrossRef] [PubMed]

17. Pichika, R.; Easwaramoorthy, B.; Christian, B.T.; Shi, B.; Narayanan, T.K.; Collins, D.; Mukherjee, J. Nicotinic α4β2 receptor imaging agents. Part III. Synthesis and biological evaluation of 3-(2-(S)-azetidinylmethoxy)-5-(3′-18F-fluoropropyl)pyridine (18F-nifzetidine). *Nucl. Med. Biol.* **2011**, *38*, 1183–1192. [CrossRef]

18. Pandey, S.K.; Pan, S.; Kant, R.; Kuruvilla, S.A.; Pan, M.L.; Mukherjee, J. Synthesis and evaluation of 3-123I-iodo-5-[2-(S)-3-pyrrolinylmethoxy]-pyridine (niodene) as a potential nicotinic α4β2 receptor imaging agent. *Bioorg Med. Chem. Lett.* **2012**, *22*, 7610–7614. [CrossRef]

19. Kuruvilla, S.A.; Hillmer, A.T.; Wooten, D.W.; Patel, A.; Christian, B.T.; Mukherjee, J. Synthesis and evaluation of 2-18F-fluoro-5-iodo-3-[2-(S)-3,4-dehydropyrrolinylmethoxy]pyridine (18F-niofene) as a potential imaging agent for nicotinic α4β2 receptors. *Am. J. Nucl. Med. Mol. Imaging* **2014**, *4*, 354–364.

20. Horti, A.G.; Gao, Y.; Kuwabara, H.; Wang, Y.; Abazyan, S.; Yasuda, R.P.; Tran, T.; Xiao, Y.; Sahibzada, N.; Holt, D.P.; et al. [18F]ASEM, a radiolabeled antagonist for imaging α7-nicotinic acetylcholine receptor (α7-nAChR) with positron emission tomography (PET). *J. Nucl. Med.* **2014**, *55*, 672–677. [CrossRef]

21. Donat, C.K.; Hansen, H.H.; Hansen, H.D.; Mease, R.C.; Horti, A.G.; Pomper, M.G.; L'Estrade, E.T.; Herth, M.M.; Peters, D.; Knudsen, G.M.; et al. In Vitro and In Vivo Characterization of Dibenzothiophene Derivatives [125I]Iodo-ASEM and [18F]ASEM as Radiotracers of Homo- and Heteromeric α7 Nicotinic Acetylcholine Receptors. *Molecules* **2020**, *25*, 1425. [CrossRef] [PubMed]

22. Hawrot, E.; Wilson, P.T.; Gershoni, J.M.; Reese, J.H.; Lentz, T.L. Alpha-bungarotoxin binding to a high molecular weight component from lower vertebrate brain identified on dodecyl sulfate protein-blots. *Brain Res.* **1986**, *373*, 227–234. [CrossRef] [PubMed]

23. Love, R.A.; Stroud, R.M.; Love, R.A.; Stroud, R.M. The crystal structure of a-bungarotoxin at 2.5A resolution: Relation to solution structure and binding to acetylcholine receptor. *Protein Eng.* **1986**, *1*, 37–46. [CrossRef] [PubMed]

24. Rasmussen, B.A.; Perry, D.C. An Autoradiographic analysis of [125I] α-bungarotoxin binding in rat brain after chronic nicotine exposure. *Neurosci. Lett.* **2006**, *404*, 9–14. [CrossRef] [PubMed]

25. Colloby, S.J.; Perry, E.K.; Pakrasi, S.; Pimlott, S.L.; Wyper, D.J.; McKeith, I.G.; Williams, E.D.; O'Brien, J.T. Nicotinic 123I-5IA-85380 single photon emission computed tomography as a predictor of cognitive progression in Alzheimer's disease and dementia with Lewy bodies. *Am. J. Geriatr. Psychiatry* **2010**, *18*, 86–90. [CrossRef]

26. Okada, H.; Ouchi, Y.; Ogawa, M.; Futatsubashi, M.; Saito, Y.; Yoshikawa, E.; Terada, T.; Oboshi, Y.; Tsukada, H.; Ueki, T.; et al. Alterations in α4β2 nicotinic receptors in cognitive decline in Alzheimer's aetiopathology. *Brain* **2013**, *136 Pt 10*, 3004–3017. [CrossRef] [PubMed]

27. Lagarde, J.; Sarazin, M.; Chauvire, V.; Stankoff, B.; Kas, A.; Lacomblez, L.; Peyronneau, M.-A.; Bottlaender, M. Cholinergic changes in aging and Alzheimer's disease. An [18F]-F-A-85380 exploratory PET study. *Alzheimer Dis. Assoc. Disord.* **2017**, *31*, 8–12. [CrossRef]

28. Coughlin, J.M.; Rubin, L.H.; Du, Y.; Rowe, S.P.; Crawford, J.L.; Rosenthal, H.B.; Frey, S.M.; Marshall, E.S.; Shinehouse, L.K.; Table 2 summarizes the affinities and selectivities for the various at the α4β2 and α7 nAChRs. The selectivity of KS7 seems to resemble nicotine, as a dual α4β2/α7 drug [43], but with significantly weaker affinities compared to nicotine. Chen, A.; et al. High availability of the a-7 nicotinic acetylcholine receptor in brains of individuals with mild cognitive impairment: A pilot study using 18F-ASEM PET. *J. Nucl. Med.* **2020**, *61*, 423–426. [CrossRef]

29. Braak, H.; Thal, D.R.; Ghebremedhin, E.; Tredici, K.D. Stages of the pathologic process in Alzheimer's disease age categories from 1 to 100 years. *J. Neuropathol. Exp. Neurol.* **2011**, *70*, 960–969. [CrossRef]

30. Liu, Q.; Huang, Y.; Shen, J.; Steffensen, S.; Wu, J. Functional α7β2 nicotinic acetylcholine receptors expressed in hippocampal interneurons exhibit high sensitivity to pathological level of amyloid β peptides. *BMC Neurosci.* **2012**, *13*, 155. [CrossRef]

31. Moretti, M.; Zoli, M.; George, A.A.; Lukas, R.J.; Pistillo, F.; Maskos, U.; Whiteaker, P.; Gotti, C. The novel α7β2-nicotinic acetylcholine receptor subtype is expressed in mouse and human basal forebrain: Biochemical and pharmacological characterization. *Mol. Pharmacol.* **2014**, *86*, 306–317. [CrossRef] [PubMed]

32. Wu, J.; Liu, Q.; Tang, P.; Mikkelsen, J.D.; Shen, J.; Whiteaker, P.; Yakel, J.L. Heteromeric α7β2 Nicotinic Acetylcholine Receptors in the Brain. *Trends Pharmacol. Sci.* **2016**, *37*, 562–574. [CrossRef]

33. Thomsen, M.S.; Zwart, R.; Ursu, D.; Jensen, M.M.; Pinborg, L.H.; Gilmour, G.; Wu, J.; Sher, E.; Mikkelsen, J.D. α7 and β2 Nicotinic Acetylcholine Receptor Subunits Form Heteromeric Receptor Complexes that Are Expressed in the Human Cortex and Display Distinct Pharmacological Properties. *PLoS ONE* **2015**, *10*, e0130572. [CrossRef] [PubMed]

34. Williams, G.; Murray, T. The role of a recently discovered alpha-7 nicotinic acetylcholine receptor on amyloid-beta pathology in Alzheimer's disease. *Alzheimer's Dement.* **2017**, *13* (Suppl. S7), P1502–P1503. [CrossRef]

35. Harel, M.; Kasher, R.; Nicolas, A.; Guss, J.M.; Balass, M.; Fridkin, M.; Smit, A.B.; Brejc, K.; Sixma, T.K.; Katchalski-Katzir, E.; et al. The binding site of acetylcholine receptor as visualized in the X-ray structure of a complex between alpha-bungarotoxin and a mimotope peptide. *Neuron* **2001**, *32*, 265–275. [CrossRef] [PubMed]

36. Schrimpf, M.R.; Sippy, K.B.; Briggs, C.A.; Anderson, D.J.; Li, T.; Ji, J.; Frost, J.M.; Surowy, C.S.; Bunnelle, W.H.; Gopalakrishnan, M.; et al. SAR of α7 nicotinic receptor agonists derived from tilorone: Exploration of a novel nicotinic pharmacophore. *Bioorg. Med. Chem. Lett.* **2012**, *22*, 1633–1638. [CrossRef]

37. Easwaramoorthy, B.; Pichika, R.; Collins, D.; Potkin, S.G.; Leslie, F.M.; Mukherjee, J. Effect of acetylcholinesterase inhibitors on nicotinic α4β2 receptor PET radiotracer, ^{18}F-Nifene: A measure of acetylcholine competition. *Synapse* **2007**, *61*, 29–36. [CrossRef]

38. Wong, D.F.; Kuwabara, H.; Pomper, M.; Holt, D.P.; Brasic, J.R.; George, N.; Frolov, B.; Willis, W.; Gao, Y.; Valentine, H.; et al. Human brain imaging of α7 nAChR with [^{18}F]ASEM: A new PET radiotracer for neuropsychiatry and determination of drug occupancy. *Mol. Imaging Biol.* **2014**, *16*, 730–738. [CrossRef]

39. Azam, L.; Winzer-Serhan, U.; Leslie, F.M. Co-expression of α7 and β2 nicotinic acetylcholine receptor subunit mRNAs within rat brain cholinergic neurons. *Neuroscience* **2003**, *119*, 965–977. [CrossRef]

40. Meeker, R.B.; Michels, K.M.; Libber, M.T.; Hayward, J.N. Characteristics and distribution of high- and low-affinity alpha bungarotoxin binding sites in the rat hypothalamus. *J. Neurosci.* **1986**, *6*, 1866–1875. [CrossRef]

41. Dickinson, J.A.; Kew, J.N.C.; Wonnacott, S. Presynaptic α7- and β2-containing nicotinic acetylcholine receptors modulate excitatotry amino acid release from rat prefrontal cortex nerve terminals via distinct cellular mechanisms. *Mol. Pharmacol.* **2008**, *74*, 348–359. [CrossRef] [PubMed]

42. Morales-Perez, C.L.; Noviello, C.M.; Hibbs, R.E. X-ray structure of the human α4β2 nicotinic receptor. *Nature* **2016**, *538*, 411–415. [CrossRef] [PubMed]

43. Crestey, F.; Jensen, A.A.; Soerensen, C.; Magnus, C.B.; Andreasen, J.T.; Peters, G.H.J.; Kristensen, J.L. Dual Nicotinic Acetylcholine Receptor α4β2 Antagonists/α7 Agonists: Synthesis, Docking Studies, and Pharmacological Evaluation of Tetrahydroisoquinolines and Tetrahydroisoquinolinium Salts. *J. Med. Chem.* **2018**, *61*, 1719–1729. [CrossRef] [PubMed]

44. Chellappan, S.K.; Xiao, Y.; Tueckmantel, W.; Kellar, K.J.; Kozikowski, A.P. Synthesis and pharmacologica evaluation of novel 9- and 10-substituted cytisine derivatives. Nicotinic ligands of enhanced subtype selectivity. *J. Med. Chem.* **2006**, *49*, 2673–2676. [CrossRef] [PubMed]

45. Campello, H.R.; Del Villar, S.G.; Honraedt, A.; Minguez, T.; Oliveria, A.S.F.; Ranaghan, K.E.; Shoemark, D.K.; Bermudez, I.; Gotti, C.; Sessions, R.B.; et al. Unlocking nicotinic selectivity via direct C-H functionalization of (−)-cytisine. *Chem* **2018**, *4*, 1710–1725. [CrossRef]

46. Whiting, P.; Lindstrom, J. Pharmacological properties of immune-isolated neuronal nicotinic receptors. *J. Neurosci.* **1986**, *6*, 3061–3069. [CrossRef] [PubMed]

47. Gao, Y.; Mease, R.C.; Olson, T.T.; Kellar, K.J.; Dannals, R.F.; Pomper, M.G.; Horti, A.G. [^{125}I]Iodo-ASEM, a specific in vivo radioligand for α7-nAChR. *Nucl. Med. Biol.* **2015**, *42*, 488–493. [CrossRef]

48. Gao, Y.; Kellar, K.J.; Yasuda, R.P.; Tran, T.; Xiao, Y.; Dannals, R.F.; Horti, A.G. Derivatives of dibenzothiophene for PET imaging of α7 nicotinic acetylcholine receptors. *J. Med. Chem.* **2013**, *56*, 7574–7589. [CrossRef]

49. Das, M.K.; Mukherjee, J. Radiosynthesis of [F-18]fluoxetine as a potential radiotracer of serotonin reuptake-sites. *Int. J. Appl. Radiat. Isot.* **1993**, *44*, 835–842. [CrossRef]

50. Mukherjee, J.; Shi, B.; Christian, B.T.; Chattopadhyay, S.; Narayanan, T.K. ^{11}C-Fallypride: Radiosynthesis and preliminary evaluation of novel dopamine D2/D3 receptor PET radiotracer in nonhuman primate brain. *Bioorganic Med. Chem.* **2004**, *12*, 95–102. [CrossRef]

51. Nguyen, G.A.H.; Liang, C.; Mukherjee, J. [^{124}I]IBETA, a new Aβ amyloid plaque PET imaging agent for Alzheimer's disease. *Molecules* **2022**, *27*, 4552. [CrossRef] [PubMed]